Preprints of the 19th World Congress
The International Federation of Automatic Control
Cape Town, South Africa. August 24-29, 2014

Sensorless Damping Control of a High Speed Flexure Guided Nanopositioner

Matthew W. Fairbairn, Sachin P. Wadikhaye and S. O. Reza Moheimani

School of Electrical Engineering and Computer Science at The University of Newcastle, Callaghan, NSW, Australia (e-mail: Reza.Moheimani@newcastle.edu.au).

Abstract:
The scan speed of the Atomic Force Microscope (AFM) is limited by the highly resonant nature of the nanopositioner which scans the sample relative to the probe tip. Feedback control may be used to dampen the resonance; however this requires external displacement sensors which may introduce high frequency noise into the feedback loop. In this work an active piezoelectric shunt control system, which requires no external feedback sensors, is designed to damp the resonance of a high speed flexure guided nanopositioner. The shunt impedance is designed in such a way that the closed loop transfer function from applied voltage to actuator displacement is equivalent to that of a displacement feedback system using a Positive Position Feedback (PPF) controller. This impedance design is an improvement over a passive impedance in that higher damping of the resonance is achievable. AFM images of a test sample were obtained to demonstrate the reduction of image artifacts when this control technique is applied.

Keywords: Microscopes, control applications, piezoelectric shunt control, nanopositioner, resonance damping.

1. INTRODUCTION

The Atomic Force Microscope (AFM), invented by Binnig et al. (1986), generates three-dimensional images of a sample surface by scanning the sample underneath a micro-cantilever which has a sharp probe tip on its underside. When operating in the constant-height contact imaging mode, see Jalili and Laxminarayana (2004), the cantilever deflection, which varies in proportion to the sample topography, is plotted as a function of the lateral scan position to produce a three-dimensional image of the sample with sub-nanometer resolution.

When imaging in this manner a limitation to scan speed is the highly resonant nature of the piezoelectric scanner which is used to scan the sample along the lateral axes (X and Y). The most common scan trajectory is the raster pattern which is produced by applying a triangular waveform to the X axis and a slow ramp or pseudo-ramp signal to the Y axis. The frequency spectrum of the triangle waveform consists of the fundamental frequency and its odd harmonics. Although the amplitude of each harmonic is inversely proportional to the square of the harmonic number it is likely that the higher order harmonics of the triangular waveform may excite the resonance of the scanner (see Croft and Devasia (1999), Moheimani (2008), and Clayton et al. (2009)) causing the scanner to vibrate. External noise may also excite this resonance. This vibration will produce ripples in the resulting image. As scan speed is increased and the frequency of the triangular waveform approaches the resonance frequency of the scanner the magnitude of these vibrations will increase. To avoid distortions in the image the fundamental frequency of the triangular signal is restricted to 1 % of the nanopositioner's first resonance frequency (see Moheimani (2008)).

The flexure based nanopositioner (see Yong et al. (2009)) consists of a platform connected to a base by several flexures. The platform on which the sample is mounted is actuated by piezoelectric stack actuators which cause the flexures to bend when they expand or contract. This design is preferred over alternative designs due to its reduced cross coupling between axes and higher mechanical bandwidth.

Feedback control is an effective way to damp the resonance of the scanner, as demonstrated in Sebastian et al. (2008), Bhikkaji and Moheimani (2008), and Mahmood and Moheimani (2009). To implement feedback control, capacitive displacement sensors are commonly used which are limited in bandwidth and prone to noise (see Moheimani (2008)) which limits the precision of the nanopositioner. The technique of piezoelectric shunt control, which uses the piezoelectric transducer for both actuation and sensing, may be used to damp the resonance of the scanner, as demonstrated in Fleming and Moheimani (2006), Aphale et al. (2007), and Eielsen and Fleming (2010) without the need for external displacement sensors. By removing the external displacement sensors the problems associated with capacitive sensors are avoided.

This work demonstrates a new approach for designing a piezoelectric shunt controller for the application of damping the first resonance mode of a high speed flexure based nanopositioner. Section 2 derives the equivalence of the piezoelectric shunt system to a displacement negative

Copyright © 2014 IFAC

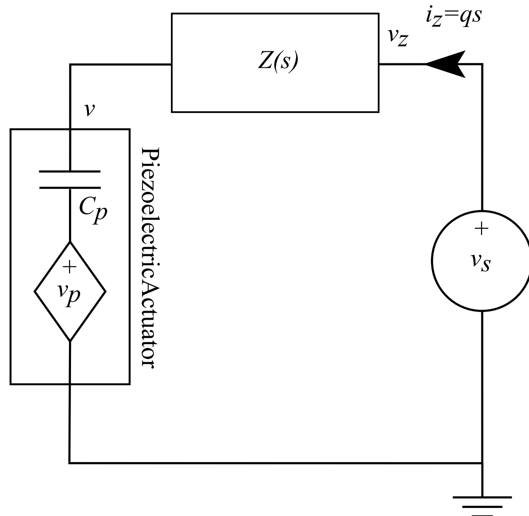

Fig. 1. Schematic of the piezoelectric shunt control system.

feedback system. In Section 3 this relationship is used to design an active impedance which allows for greater damping than is possible with previous shunt controller designs. The efficacy of this controller is demonstrated experimentally in Section 6.

2. PIEZOELECTRIC SHUNT CONTROL

A piezoelectric transducer may be modeled as a dependent voltage source v_p in series with a capacitance C_p, as discussed in Dosch et al. (1992). When the transducer is subject to a strain, a voltage v_p is generated according to the relationship $v_p = \alpha d$, where α is the actuator voltage to displacement coefficient and d is the actuator displacement. This ability of a piezoelectric transducer to convert mechanical energy to electrical energy and *vice versa* is the basis of piezoelectric shunt control. An electrical impedance $Z(s)$ is placed in series with the driving signal v_s, as shown in Fig. 1. The charge q generated as a result of a strain caused by actuator displacement, due to v_s or a disturbance strain w, flows through $Z(s)$ to produce a counteractive voltage v_z. By tuning the parameters of $Z(s)$, v_z may be optimized to damp the resonance of the actuator.

A block diagram of the piezoelectric shunt control system is shown in Fig. 2, where the piezoelectric transducer is modeled as a two-input two-output system $G(s)$. The inputs are the voltage applied across the piezoelectric transducer terminals v and a disturbance strain w. The outputs are the actuator displacement d and the charge q generated by the transducer. In this representation v_z is the voltage across the shunt impedance and d_w is the initial actuator displacement due to a disturbance. The transfer function from v to d is modeled as

$$G_{dv}(s) = \frac{d(s)}{v(s)} = \frac{\beta_v \omega_n^2}{s^2 + \omega_n \zeta s + \omega_n^2}, \tag{1}$$

and the transfer function from w to d_w is is modeled as

$$G_{d_w w}(s) = \frac{d_w(s)}{w(s)} = \frac{\beta_w \omega_n^2}{s^2 + \omega_n \zeta s + \omega_n^2}, \tag{2}$$

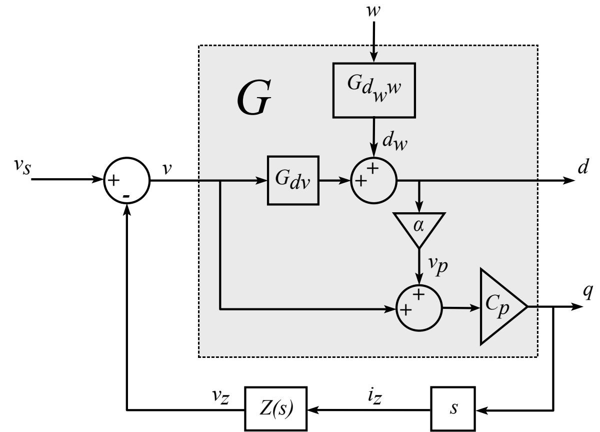

Fig. 2. Block diagram of the piezoelectric shunt control system.

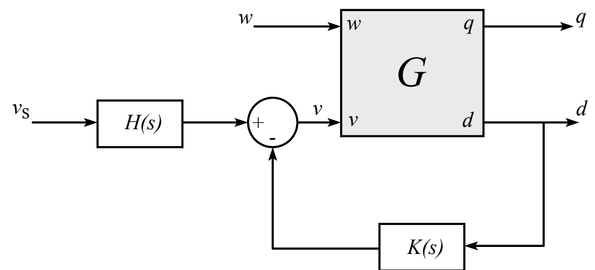

Fig. 3. Equivalent displacement feedback loop of the piezoelectric shunt control system.

where ω_n is the natural frequency of the actuator, β_v and β_w are the steady state gains of $G_{dv}(s)$ and $G_{d_w w}(s)$ respectively, and ζ is the damping coefficient.

The transfer function from the applied voltage v_s to displacement d is determined to be (see Fairbairn et al. (2011))

$$G_{dv_s}(s) = \frac{H(s)G_{dv}(s)}{1 + K(s)G_{dv}(s)}, \tag{3}$$

where

$$K(s) = \frac{sZ(s)C_p\alpha}{1 + sZ(s)C_p}, \tag{4}$$

and

$$H(s) = \frac{1}{1 + sZ(s)C_p}. \tag{5}$$

In this form $G_{dv_s}(s)$ is equivalent to a displacement negative feedback loop with a controller $K(s)$ and a pre-filter $H(s)$ as shown in Fig. 3. The pre-filtering effect is due to the electrical dynamics of the shunt circuit. This pre-filtering effect will distort the frequency response from the applied voltage to displacement. To track the reference signal it is necessary to filter the reference signal by $H^{-1}(s)$.

The transfer function from a disturbance to the actuator displacement was determined to be (see Fairbairn et al. (2011))

$$G_{dw}(s) = \frac{G_{d_w w}(s)}{1 + K(s)G_{dv}(s)}, \tag{6}$$

which is not affected by the prefilter $H(s)$.

3. DESIGN OF AN ACTIVE SHUNT IMPEDANCE

For a passive shunt impedance consisting of an inductance in series with a resistance ($Z(s) = Ls + R$) designed for the system shown in Fig. 1 the equivalent displacement feedback controller is

$$K(s) = \frac{\alpha s \left(s + \frac{R}{L}\right)}{s^2 + \frac{R}{L}s + \frac{1}{C_p L}}, \quad (7)$$

which is a resonant controller (see Fairbairn and Moheimani (2012)). The gain of this controller is limited by the voltage to displacement coefficient of the piezoelectric transducer and the passive nature of the impedance. To increase the gain of the controller, and consequently the damping of the system, an active impedance (see Fleming and Moheimani (2005)), which can supply energy to the system, must be used.

In this work an active impedance was designed in such a way that the equivalent displacement feedback controller is a Positive Position Feedback (PPF) controller with a transfer function

$$K(s) = \frac{a}{s^2 + 2\zeta_c \omega_c s + \omega_c^2}, \quad (8)$$

where a and ζ_c are control design parameters which determine the gain at the frequency of interest ω_c (ω_c is set close to ω_n) and the bandwidth of control. The transfer function of the PPF controller rolls off at a rate of 40 dB/decade for high frequencies which makes the closed loop system robust to spillover effects on unmodeled high frequency actuator dynamics.

The controller gain is no longer limited by the voltage to displacement coefficient of the piezoelectric transducer and may be increased as needed by tuning the equivalent shunt impedance.

The equivalent shunt impedance transfer function for the PPF controller can be determined by rearranging (4) in the form

$$Z(s) = \frac{K(s)}{sC_p(\alpha - K(s))}. \quad (9)$$

Substituting (8) in (9) results in the transfer function

$$Z_{PPF}(s) = \frac{1}{s} . \frac{a}{\alpha C_p s^2 + 2\alpha C_p \zeta_c \omega_c s + \alpha C_p \omega_c^2 - aC_p}. \quad (10)$$

It can easily be proven that $Z_{PPF}(s)$ is an active impedance by showing that the transfer function is not positive real (see Bai and Freund (2000)).

4. PHYSICAL REALIZATION OF THE PIEZOELECTRIC SHUNT CONTROL SYSTEM

The active impedance was implemented synthetically (see Fleming et al. (2000)) by measuring the terminal current $i_z(s)$ and controlling the terminal voltage $v_z(s)$ according to the relationship $v_z(s) = i_z(s)Z(s)$.

The piezoelectric actuator must be driven by a high voltage amplifier. The amplifier chosen for this work is the

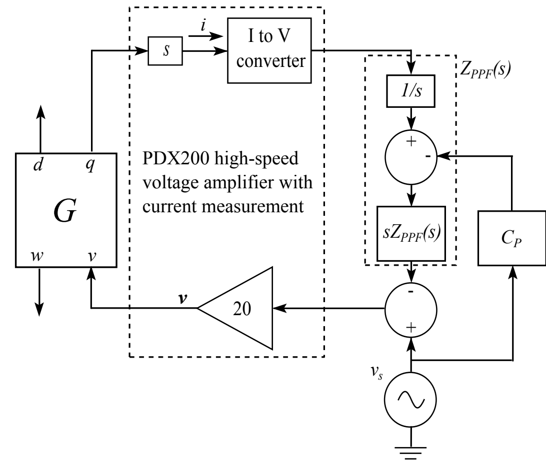

Fig. 4. Implementation of a synthetic impedance with the pre-filter $H^{-1}(s)$ for reference tracking.

PDX200 high speed voltage amplifier, manufactured by Piezodrive. (2013), which has a gain of 20. In addition it has a current monitor output which provides a voltage proportional to the current flowing through the piezoelectric transducer (1V/A). This makes it relatively straightforward to implement the synthetic impedance as shown in Fig. 4. The current is measured by the current monitor of the PDX200 voltage amplifier which has an inbuilt I to V converter. This voltage output is then passed into a filter implementing the transfer function Z_{PPF}.

The filter $Z_{PPF}(s)$ was implemented with a state variable filter using operational amplifiers, as the high resonance frequency of the scanner limits the number of Digital Signal Processor (DSP) options due to sampling constraints.

Note the inclusion of the feedforward gain C_p in Fig. 4. As mentioned in Section 2, the reference signal must be pre-filtered by $H^{-1}(s)$ to compensate for the electrical dynamics of the shunt impedance. The transfer function of $H^{-1}(s)$ is

$$H^{-1}(s) = 1 + sZ(s)C_p, \quad (11)$$

which is non-causal and therefore may be difficult to implement. By separating the integrator in $Z_{PPF}(s)$, $H^{-1}(s)$ may be implemented by adding the feedforward gain C_p.

5. SYSTEM MODELING

A high-speed flexure-guided nanopositioner was used in this work to demonstrate the proposed control technique. The device consists of a moving platform suspended by several flexures and actuated by a 5 mm × 5 mm × 10 mm piezoelectric stack actuator in the X and Y directions. A full description of the nanopositioner is provided in Yong et al. (2013) and Yong and Moheimani (2013). A MicroSense 6810 capacitive sensor was used to measure the displacement of the nanopositioner for modeling and confirmation of results. The sensitivity of the capacitive sensors is 2.5 μm/V.

To demonstrate the active piezoelectric shunt control technique the shunt control system was applied to the X axis of the nanopositioner.

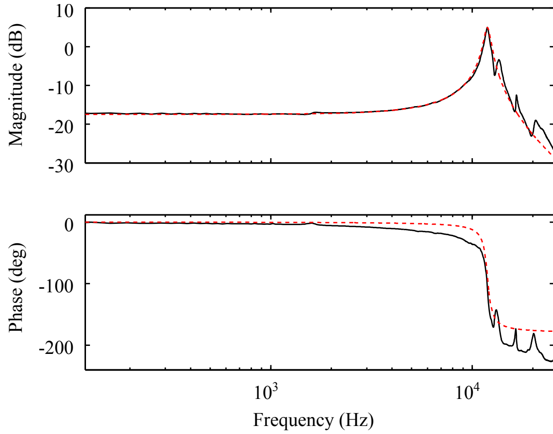

Fig. 5. Open loop frequency response of the nanopositioner X axis (- -) and the fitted model (—).

A chirp signal was applied to the actuator and the resulting frequency response was measured with a Stanford Research Systems SR785 Dynamic Signal Analyzer. The open loop frequency response is shown in Fig. 5. A second order model was fitted to the measured frequency response as shown in Fig. 5. Note that the delay associated with the capacitive displacement sensor is ignored. The fitted transfer function is

$$G_{dv} = \frac{300}{s^2 + 5700s + 5.595 \times 10^9}. \tag{12}$$

C_P was measured to be 307 nF. α was determined by measuring the admittance transfer function G_{iv}.

$$G_{iv} = \alpha C_P G_{dv} s + C_P s. \tag{13}$$

To measure G_{iv} a voltage was applied to the piezoelectric actuator and the resulting current was measured. The measured transfer function was

$$G_{iv} = \frac{3.125 \times 10^{-7} s^3 + 0.001781 s^2 + 1795 s}{s^2 + 5700s + 5.595 \times 10^9} \tag{14}$$

Solving for α in (13) gives a value of $\alpha = 750000$.

The shunt impedance was tuned experimentally to damp the first resonance of the X axis below that of the next uncontrolled resonance. This resulted in a 13.9 dB reduction in the resonance peak as shown in Fig. 6.

The frequency response of the tuned shunt impedance was measured to obtain the transfer function

$$Z_{PPF}(s) = \frac{-1.52 \times 10^{16}}{s^3 + 1.52 \times 10^4 s^2 + 1.029 \times 10^{10} s}. \tag{15}$$

Substituting (15) into (4) gives the equivalent displacement feedback PPF controller

$$K(s) = \frac{-3.5 \times 10^{15}}{s^2 + 1200s + 5.625 \times 10^9}. \tag{16}$$

6. IMAGING PERFORMANCE

Images of an ASM 750-HD (see ASM (2013)) calibration specimen were obtained in open loop and closed loop to evaluate the performance of the proposed controller. The ASM 750-HD calibration specimen is composed of nickel and has features with a height of 100 nm and a pitch

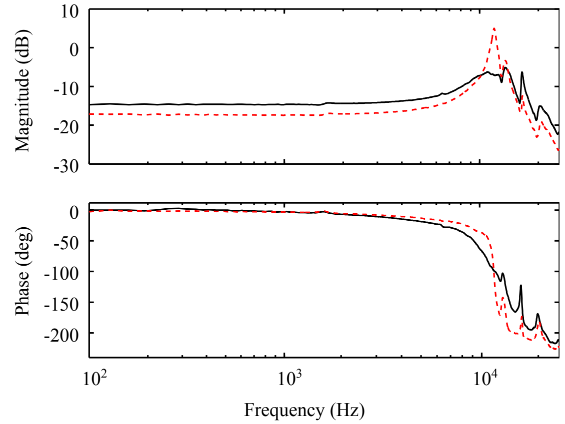

Fig. 6. Open loop (- -) and closed loop (—) frequency response of the nanopositioner X axis. A 13.9 dB reduction in the resonance peak was achieved.

of 738 nm. A Nanosurf EasyScan 2 AFM (see Nanosurf (2013)) was used to obtain the images. The Nanosurf EasyScan 2 nanopositioner was replaced with the high speed nanopositioner described in Section 5. The AFM was operated in the constant-height contact imaging mode.

A slow ramp signal was applied to the Y axis of the nanopositioner with a 500 Hz triangular signal applied to the X axis to produce the raster pattern for scanning the sample. Fig. 7(a) shows the measured displacement and the reference signal. Oscillations in the measured displacement signal are clearly visible and the resulting image artifacts may be seen in the AFM images of Fig. 8(a) and 9(a). When the piezoelectric shunt control is applied to the system these oscillations no longer appear in the measured displacement signal (Fig. 7(b)) or the sample images of Fig. 8(b) and 9(b).

6.1 Hysteresis

The measured displacement signals shown in Fig. 7(a) and Fig. 7(b) show significant hysteresis (see Adriaens et al. (2000)). This hysteresis results in a curvature of the image features as can be seen in Figs. 8(a), 9(a), 8(b) and 9(b). The two most common techniques for hysteresis compensation are model based feedforward control (see Leang et al. (2009)) and closed-loop tracking control (see Fleming et al. (2010)). Keeping the essence of sensorless control, a feedforward approach was used to mitigate the hysteretic nonlinearity and enhance tracking performance.

The measured displacement should be a triangular signal. An input triangular signal in Fourier series form can be written as

$$r(t) = \sum_{k=1}^{\infty} A_k sin(\omega_k t), \tag{17}$$

where $A_k = \frac{8}{\pi^2 k^2} sin(\frac{\pi k}{2})$ and $\omega_k = 2\pi k f$, with f being the fundamental frequency of the triangular waveform. To eliminate the hysteretic effects in the output, instead of using a triangular wave, inputs to the actuator are shaped such that the output is a triangular waveform. In other words, the amplitude and phase of harmonics are rectified as per the system characterization such that a pseudo triangular waveform is obtained as:

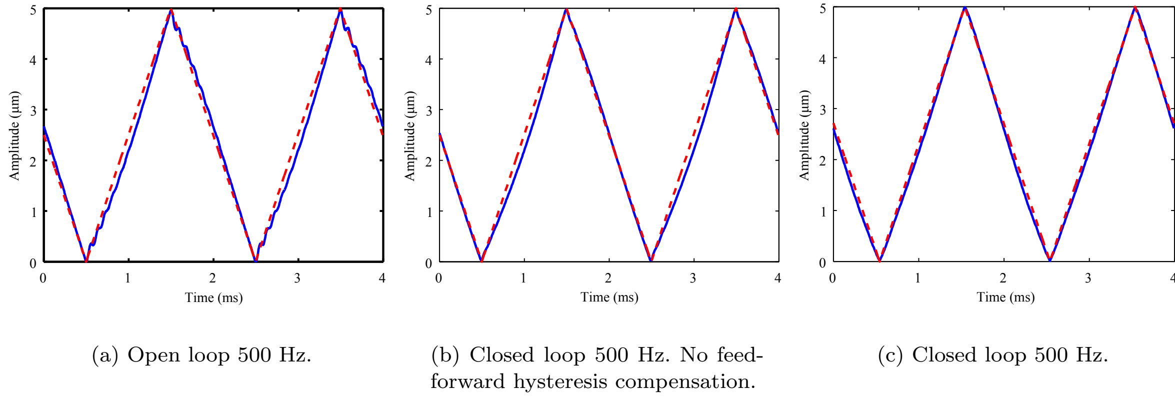

(a) Open loop 500 Hz.

(b) Closed loop 500 Hz. No feedforward hysteresis compensation.

(c) Closed loop 500 Hz.

Fig. 7. Measured X axis displacement (—) and reference signal (- - -).

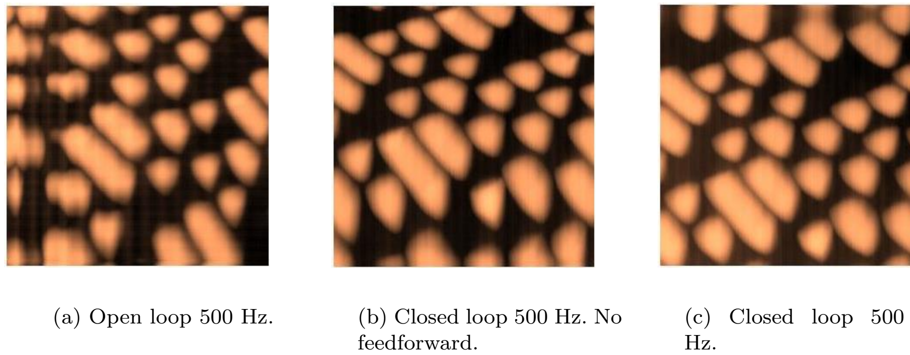

(a) Open loop 500 Hz.

(b) Closed loop 500 Hz. No feedforward.

(c) Closed loop 500 Hz.

Fig. 8. Obtained 2D images of the ASM 750-HD calibration specimen. The scan area is 5 μm × 5 μm.

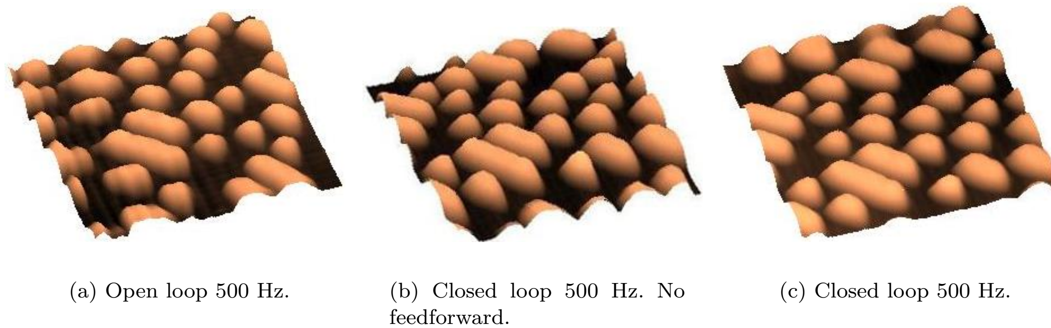

(a) Open loop 500 Hz.

(b) Closed loop 500 Hz. No feedforward.

(c) Closed loop 500 Hz.

Fig. 9. Obtained 3D images of the ASM 750-HD calibration specimen.. The scan area is 5 μm × 5 μm.

$$u(t) = \sum_{k=1}^{\infty} \frac{A_k}{|G_{dv_s}(i\omega_k)|} sin(\omega_k t - \phi_k), \quad (18)$$

where $k = 1, 2, ...$

Here, the phase angle ϕ_k is a combination of a linear component $\angle G_{dv_s}(i\omega_k)$ and a hysteretic component Λ_k. The linear component is obtained from the small amplitude frequency response of the nanopositioner, while, the hysteretic component is approximated at a phase shift (see Cruz-Hernandez and Hayward (2001)).

Figs. 7(c), 8(c) and 9(c) demonstrate the reduction in hysteresis when this shaped signal is applied. An integral tracking controller would give better tracking performance but this would require the nanopositioner displacement to be measured. As the piezoelectric shunt control system may be seen to emulate a displacement negative feedback loop the nanopositioner displacement may be extracted by designing the shunt impedance with this in mind. Future work will involve measuring the nanopositioner displacement in this manner and applying an integral controller to this signal for tracking.

7. CONCLUSION/FURTHER WORK

In this work the technique of active piezoelectric shunt control was applied to a high speed flexure guided nanoposi-

tioner to damp the first resonance mode in the X axis. Using an active impedance rather than a passive impedance allows for a greater amount of damping to be obtained. Damping the first resonant mode of the nanopositioner X axis enabled fast scan speeds with reduced image artifacts due to scan induced vibration.

Using feedforward control to compensate for hysteresis demonstrated that further improvements in image quality may be achieved. Adding a tracking control feedback loop with integral action would reduce the hysteresis further. Future research will focus on measuring the displacement of the piezoelectric shunt controlled transducer to enable such a control loop to be implemented.

ACKNOWLEDGEMENTS

The authors would like to thank Dr. Yuen Yong for her technical advice. This work was supported by the Australian Research Council.

REFERENCES

Adriaens, De Koning, W.L., and Banning, R. (2000). Modeling piezoelectric actuators. *IEEE/ASME Transactions on Mechatronics*, 5(4), 331–341.

Aphale, S., Fleming, A.J., and Moheimani, S.O.R. (2007). High speed nano-scale positioning using a piezoelectric tube actuator with active shunt control. *Micro and Nano Letters*, 2(1), 9–12.

ASM (2013). Advanced surface microscopy inc. website. URL `http://www.asmicro.com`.

Bai, Z. and Freund, R. (2000). Eigenvalue-based characterization and test for positive realness of scalar transfer functions. *Automatic Control, IEEE Transactions on*, 45(12), 2396–2402.

Bhikkaji, B. and Moheimani, S.O.R. (2008). Integral resonant control of a piezoelectric tube actuator for fast nano-scale positioning. *IEEE/ASME Transactions on Mechatronics*, 13(5), 530–537.

Binnig, G., Quate, C.F., and Gerber, C. (1986). Atomic force microscope. *Physical Review Letters*, 56(9), 930.

Clayton, G.M., Tien, S., Leang, K.K., and Zou, Q. (2009). A review of feedforward control approaches in nanopositioning for high-speed spm. *Journal of Dynamic Systems, Measurement, and Control.*

Croft, D. and Devasia, S. (1999). Vibration compensation for high speed scanning tunneling microscopy. *Review of Scientific Instruments*, 70(12), 4600–4605.

Cruz-Hernandez, J. and Hayward, V. (2001). Phase control approach to hysteresis reduction. *Control Systems Technology, IEEE Transactions on*, 9(1), 17–26. doi: 10.1109/87.896742.

Dosch, J.J., Inman, D.J., and Garcia, E. (1992). A Self-Sensing Piezoelectric Actuator for Collocated Control. *Journal of Intelligent Material Systems and Structures*, 3, 166–185. doi:10.1063/1.109413.

Eielsen, A.A. and Fleming, A.J. (2010). Passive shunt damping of a piezoelectric stack nanopositioner. In *Proc. American Control Conference*, 4963–4968. Baltimore, MD.

Fairbairn, M.W. and Moheimani, S.O.R. (2012). Resonant control of an atomic force microscope micro-cantilever for active q control. *Review of Scientific Instruments*, 83(8), 083708 (9pp).

Fairbairn, M.W., Moheimani, S.O.R., and Fleming, A.J. (2011). Q-control of an atomic force microscope microcantilever: A sensor-less approach. *IEEE/ASME Journal of Microelectromechanical Systems*, 20(6), 1372 – 1381.

Fleming, A.J., Aphale, S., and Moheimani, S.O.R. (2010). A new method for robust damping and tracking control of scanning probe microscope positioning stages. *IEEE Transactions on Nanotechnology*, 9(4), 438–448.

Fleming, A.J., Behrens, S., and Moheimani, S.O.R. (2000). Synthetic impedance for implementation of piezoelectric shunt damping circuits. *Electronics Letters*, 36(18), 1525–1526.

Fleming, A.J. and Moheimani, S.O.R. (2005). Control oriented synthesis of high performance piezoelectric shunt impedances for structural vibration control. *IEEE Transactions on Control Systems Technology*, 13(1), 98–112.

Fleming, A.J. and Moheimani, S.O.R. (2006). Sensorless vibration suppression and scan compensation for piezoelectric tube nanopositioners. *IEEE Transactions on Control Systems Technology*, 14(1), 33–44.

Jalili, N. and Laxminarayana, K. (2004). A review of atomic force microscopy imaging systems: application to molecular metrology and biological sciences. *Mechatronics*, 14(8), 907 – 945. doi: 10.1016/j.mechatronics.2004.04.005.

Leang, K.K., Zou, Q., and Devasia, S. (2009). A review of feedforward control approaches in nanopositioning for high-speed spm. *Journal of dynamic systems, measurement, and control*, 131, 061101–1.

Mahmood, I.A. and Moheimani, S.O.R. (2009). Making a commercial atomic force microscope more accurate and faster using positive position feedback control. *Review of Scientific Instruments*, 80(6), 063705.

Moheimani, S.O.R. (2008). Invited review article: Accurate and fast nanopositioning with piezoelectric tube scanners: Emerging trends and future challenges. *Review of Scientific Instruments*, 79(7). Article Number: 071101.

Nanosurf (2013). Nanosurf website. URL `http://www.nanosurf.com`.

Piezodrive. (2013). Piezodrive website. URL `http://www.piezodrive.com`.

Sebastian, A., Pantazi, A., Moheimani, S.O.R., Pozidis, H., and Eleftheriou, E. (2008). Achieving subnanometer precision in a mems-based storage device during self-servo write process. *Nanotechnology, IEEE Transactions on*, 7(5), 586–595. doi: 10.1109/TNANO.2008.926441.

Yong, Y.K., Aphale, S., and Moheimani, S.O.R. (2009). Design, identification and control of a flexure-based XY stage for fast nanoscale positioning. *IEEE Transactions on Nanotechnology*, 8(1), 46–54.

Yong, Y.K., Bhikkaji, B., and Moheimani, S.O.R. (2013). Design, Modeling and FPAA-based Control of a High-speed Atomic Force Microscope Nanopositioner. *IEEE/ASME Transactions on Mechatronics*, 18(3), 1060–1071.

Yong, Y.K. and Moheimani, S.O.R. (2013). Design of an Inertially Counterbalanced Z-nanopositioner for High-Speed Atomic Force Microscopy. *IEEE Transactions on Nanotechnology*, 12(2), 137–145.